

Charge structure factors of doped armchair nanotubes in the presence of electron-phonon interaction

Hamed Rezania, Farshad Azizi

Citation: Chin. Phys. B . 2020, 29(9): 096501 . **doi:** 10.1088/1674-1056/ab942e
Journal homepage: http://cpb.iphy.ac.cn; http://iopscience.iop.org/cpb

What follows is a list of articles you may be interested in

Alkyl group functionalization-induced phonon thermal conductivity attenuation in graphene nanoribbons

Caiyun Wang(王彩云), Shuang Lu(鲁爽), Xiaodong Yu(于晓东), Haipeng Li(李海鹏)
Chin. Phys. B . 2019, 28(1): 016501 . **doi:** 10.1088/1674-1056/28/1/016501

Temperature-induced effect on refractive index of graphene based on coated in-fiber Mach-Zehnder interferometer

Li-Jun Li(李丽君), Shun-Shun Gong(宫顺顺), Yi-Lin Liu(刘仪琳), Lin Xu(徐琳), Wen-Xian Li(李文宪), Qian Ma(马茜), Xiao-Zhe Ding(丁小哲), Xiao-Li Guo(郭晓丽)
Chin. Phys. B . 2017, 26(11): 116504 . **doi:** 10.1088/1674-1056/26/11/116504

Structural and optical properties of thermally reduced graphene oxide for energy devices

Ayesha Jamil, Faiza Mustafa, Samia Aslam, Usman Arshad, Muhammad Ashfaq Ahmad
Chin. Phys. B . 2017, 26(8): 086501 . **doi:** 10.1088/1674-1056/26/8/086501

Kernel polynomial representation for imaginary-time Green's functions in continuous-time quantum Monte Carlo impurity solver

Li Huang(黄理)
Chin. Phys. B . 2016, 25(11): 117101 . **doi:** 10.1088/1674-1056/25/11/117101

Thermal transport properties of defective graphene： A molecular dynamics investigation

Yang Yu-Lin, Lu Yu
Chin. Phys. B . 2014, 23(10): 106501 . **doi:** 10.1088/1674-1056/23/10/106501

Charge structure factors of doped armchair nanotubes in the presence of electron–phonon interaction

Hamed Rezania† and Farshad Azizi

Department of Physics, Razi University, Kermanshah, Iran

(Received 17 April 2020; revised manuscript received 13 May 2020; accepted manuscript online 19 May 2020)

We present the behaviors of both dynamical and static charge susceptibilities of doped armchair nanotubes using the Green function approach in the context of Holstein-model Hamiltonian. Specially, the effects of magnetization and gap parameter on the the plasmon modes of armchair nanotube are investigated via calculating correlation function of charge density operators. Random phase approximation has been implemented to find the interacting dynamical charge susceptibility. The electrons in this systems interacts with each other by mediation of dispersionless Holstein phonons. Our results show that the increase of gap parameter leads to decreasing intensity of charge collective mode. Also the frequency position of the collective mode tends to higher frequencies due to the gap parameter. Furthermore the number of collective excitation mode decreases with chemical potential in the presence of electron–phonon interaction. Finally the temperature dependence of static charge structure factor of armchair nanotubes is studied. The effects of the gap parameter, magnetization and electron–phonon interaction on the static structure factor are addressed in details.

Keywords: armchair nanotube, Green's function

PACS: 65.80.Ck, 71.10.Fd, 71.22.+i **DOI:** 10.1088/1674-1056/ab942e

1. Introduction

The field of nanotubes has strongly benefited from this broad fundamental and technological interest. These nanoscale graphitic structures are of great interest for both theoretical and experimental solid state physicists in the past two decades.[1] These materials[1,2] are formed from carbon atoms arranged on rolled honeycomb lattice as cylindrical structures with nanometer diameters and micrometer lengths. Nanotubes are considered as either single molecules or quasi one-dimensional crystals with translational periodicity along the tube axis. A single wall carbon nanotube (SWCNT) is predicted to be either a metal or a semiconductor, depending on its radius and chirality.[2] Nanotubes are also mechanically very stable and strong, and their carrier mobility is equivalent to that of good metals, suggesting that they would make ideal interconnects with remarkable transport properties in nano-sized devices.[3,4] One of the significant transport properties of CNTs has been the high values of electrical conduction of CNTs, which leads to attracting considerable attention.[5] Negative differential resistance behavior of silicon monatomic chain encapsulated in carbon nanotubes has been reported.[6]

In practice, metallic carbon nanotubes are very good conductors exhibiting ballistic transport properties.[7] Simple circuits based on semiconducting carbon nanotube field effect transistors have already been demonstrated.[8] Mobility of electrons can be as high as 79000 $cm^2/V{\cdot}s$ at room temperature for semiconducting CNT field effect transistors with channel lengths of more than 300 μm.[9] Therefore understanding the mechanisms of reduction of electron mobility due to various scattering effects by simulating the nanotubes can be considered as a novel topic.

Lattice displacements due to the ripple structures are symmetric with respect to their close carbon atoms and couple to the carrier densities. The electrons moving through the sheet are coupled to the out-of-plane phonons and therefore the electron–phonon coupling play an important role in the transport properties.[10–12] The symmetric property of this displacement with respect to their neighboring atoms leads to coupling between electronic density and this mode of phonons.[13] The out of plane vibrations are dispersionless and couple with electrons in the context of Holstein-model Hamiltonian.[14,15] In this model the coupling of electrons to dispersionless optical phonons is essentially local. The electron–phonon coupling has been carefully examined and has been shown to give rise to Kohn anomalies in the phonon dispersion at edge points in the Brillioun zone where the phonon can be studied by Raman spectroscopy.[16,17] The effect of the electron–phonon coupling on the local density of states of zig-zag graphene ribbons has been studied by Sasaki *et al.*[18]

The collective charge excitation of electronic systems can be found by studying the frequency dependence of dynamical charge susceptibility. It is worthwhile to explain the experimental interpretation of imaginary part of dynamical charge susceptibility. Slow massive charged particles scatter from solids via electrical interaction in which the electric charge beam interacts with the electric charge of electrons in the solid.[19] The inelastic cross section for charged particles scattering from the electronic system can be expressed in terms of

†Corresponding author. E-mail: rezania.hamed@gmail.com

© 2020 Chinese Physical Society and IOP Publishing Ltd

charge density correlation functions. Therefore the differential inelastic cross section $\mathrm{d}^2\sigma/\mathrm{d}\Omega\,\mathrm{d}\omega$ is proportional to imaginary part of charge susceptibility. Here ω denotes the energy loss of massive charged beam which is defined as the difference between incident and scattered particles energies. Ω introduces solid angle of scattered particles. The frequency position of peaks in $\mathrm{d}^2\sigma/\mathrm{d}\Omega\,\mathrm{d}\omega$ determines the collective charge excitation spectrum of the electronic system.

In an experimental study, the strongly coupled plasmon-phonon mode dispersion has been measured by the angle-resolved reflection electron-loss spectroscopy and it was found that the discrepancy arises from electron–phonon coupling.[20] The electron–phonon coupling is the macroscopic coupling between the electronic collective modes and the optical phonons. The mode coupling phenomenon, which hybridizes the collective plasmon modes of the electron with the optical-phonon modes of the lattice, gives rise to the coupled plasmon-phonon modes which have been extensively studied[21–23] both experimentally and theoretically in bulk and two-dimensional electron systems.

In order to study electronic properties of electron gas in the nano structures and graphene, the dynamical polarizability whereby the screening effects have been found is required.[24,25] The static structure factor at fermi wave vector that gives the Thomas–Fermi screening length is important for transport properties of two-dimensional graphene.[26,27] The dynamical polarizability renormalizing the phononic Green's function can explain the phonon softening and Kohn anomlay phenomenon[28] at the Γ point. The charge response function was studied for gapped graphene[29] and graphene in the presence of magnetic field.[30] A semi-analytical expression for the dynamical density-density linear response function of doped graphene sheet within Dirac approximation at finite temperature has been performed.[31] Their results demonstrated that the fluctuations of density in bilayer case can present either single-component massive-chiral character or standard two layer character, depending on energy and doping.

The goal of this work is to study the effects of next nearest neighbor hopping amplitude, gap parameter and electron–phonon coupling on plasmon frequencies of doped armchair nanotubes at finite temperature. In order to obtain these collective modes, we study the frequency dependence of dynamical charge susceptibility due to magnetization, electron–phonon coupling strength and gap parameter in the context of Holstein-model Hamiltonian. Green's function approach has been implemented to calculate the charge susceptibility, i.e. the time ordered charge density correlation. In order to obtain the behaviors of both dynamical and static charge susceptibilities, the interacting electron–electron Green function is employed by using one loop approximation in the context of full band approach for making electronic self-energy. The frequency positions of sharp peak in dynamical charge susceptibility introduce the collective plasmonic oscillations of the above-mentioned nanostructure due to electron–phonon interaction effects. Furthermore the temperature dependence of static charge susceptibility of armchair nanotubes due to variation of magnetization and gap parameter is studied. The effects of the gap parameter on the behavior of static and dynamical charge susceptibilities have been focused. Finally we discuss and analyze our results to show how next nearest neighbor hopping, electron–phonon coupling and gap parameter affect the frequency of collective modes.

2. Theoretical formalism

The electronic properties of interaction between tight binding electrons and dispersionless local vibrational modes in graphene-like structures can be described by the Holstein-model Hamiltonian. To calculate the electronic properties of the graphene-like nanotube, we consider monolayer graphene which is folded along armchair direction. The lattice structure of each graphene layer has been shown in Fig. 1. The primitive unit cell vectors are given as follows:

$$\boldsymbol{a}_1 = \frac{a\sqrt{3}}{2}\boldsymbol{i} + \frac{a\boldsymbol{j}}{2}, \quad \boldsymbol{a}_2 = \frac{a\sqrt{3}}{2}\boldsymbol{i} - \frac{a\boldsymbol{j}}{2}, \tag{1}$$

where $\boldsymbol{i}$ and $\boldsymbol{j}$ are unit cell vectors along zigzag and armchair directions, respectively. Also the length of unit cell vectors is considered to be a. We consider electrons in π orbital of carbon atoms by using the tight-binding Hamiltonian in addition to the effect of the electron–phonon coupling due to localized phonons. An intrinsic magnetic magnetization M has been considered to be perpendicular to the axis of the nanotube. In order to obtain electrical transport properties of graphene-like nanotubes we must first examine the band structure and provide the expression for the electronic Green function. We start from a tight binding model incorporating nearest and next nearest neighboring hopping terms. A finite difference between on-site energies of two different sublattice atoms of honeycomb structure has been applied in the model Hamiltonian. Since there is magnetic long range ordered phase for graphene sheet, the contribution of electrons with $\sigma = \uparrow$ is different from that of electrons with $\sigma = \downarrow$. Thus the spin quantum number is eliminated in the following relations. The spin dependent next nearest neighbor Holstein-model Hamiltonian for monolayer graphene, H, is given by

$$\begin{aligned} H \;=\; & -t\sum_{\boldsymbol{k},\sigma}(\phi_{\boldsymbol{k}}a^{\dagger}_{\boldsymbol{k},\sigma}b_{\boldsymbol{k},\sigma} + \text{h.c.}) \\ & + g\sum_{\boldsymbol{k},\boldsymbol{q},\sigma}(a^{\dagger}_{\boldsymbol{k}+\boldsymbol{q},\sigma}a_{\boldsymbol{k},\sigma} + b^{\dagger}_{\boldsymbol{k}+\boldsymbol{q},\sigma}b_{\boldsymbol{k},\sigma})(c_{\boldsymbol{k}} + c^{\dagger}_{-\boldsymbol{k}}) \\ & + \sum_{\boldsymbol{k}}\omega_0 c^{\dagger}_{\boldsymbol{k}}c_{\boldsymbol{k}} + \sum_{\boldsymbol{k},\sigma}(\Delta a^{\dagger}_{\boldsymbol{k},\sigma}a_{\boldsymbol{k},\sigma} - \Delta b^{\dagger}_{\boldsymbol{k},\sigma}b_{\boldsymbol{k},\sigma}) \\ & - \sum_{\boldsymbol{k},\sigma}\mu_{\sigma}(a^{\dagger}_{\boldsymbol{k},\sigma}a_{\boldsymbol{k},\sigma} + b^{\dagger}_{\boldsymbol{k},\sigma}b_{\boldsymbol{k},\sigma}), \end{aligned}$$

$$\phi_{\boldsymbol{k}} = 1+\cos(k_y/2)\exp(-\mathrm{i}k_x\sqrt{3}/2), \quad (2)$$

where $a^{\dagger}_{\boldsymbol{k},\sigma}$ ($b^{\dagger}_{\boldsymbol{k},\sigma}$) creates an electron at sublattice A (B) with wave vector $\boldsymbol{k}$ and with spin quantum number σ. The wave vector $\boldsymbol{k}$ belongs to the first Brillouin zone of honeycomb lattice. Also, t is the nearest neighbor hopping integral for itinerant electrons on honeycomb lattice;[2] μ_σ introduces the spin dependent chemical potential for electron gas which is determined in the following. Moreover, $c_{\boldsymbol{k}}$ denotes the annihilation phonon operator at wave vector $\boldsymbol{k}$ on each sublattice; ω_0 refers to the frequency of the out of plane vibrations of the optical phonon of each atom on the lattice. The electron phonon couplings for sublattices A and B are determined by g. The sublattice symmetry breaking mechanism is understood as different on-site energies for A and B sublattices, namely Δ and $-\Delta$ in Eq. (2). The Fourier transformations for fermionic operators $a^{\dagger}_i$ and $b^{\dagger}_i$ can be given by

$$a^{\dagger}_{\boldsymbol{k}} = \frac{1}{\sqrt{N}}\sum_i \mathrm{e}^{-\mathrm{i}\boldsymbol{k}.\boldsymbol{R}_i}a^{\dagger}_i, \quad b^{\dagger}_{\boldsymbol{k}} = \frac{1}{\sqrt{N}}\sum_i \mathrm{e}^{-\mathrm{i}\boldsymbol{k}.\boldsymbol{R}_i}b^{\dagger}_i, \quad (3)$$

where N is the number of unit cells, $\boldsymbol{R}_i$ introduces the position vector of i th unit cell in graphene layer; $\boldsymbol{k}$ is wave vector belonging to the first Brillouin zone of nanotube structure. Depending on the zigzag or armchair type of nanotube, the region of wave vectors $\boldsymbol{k}$ are determined. Nanotubes of the type (n,n) are called armchair tubes, because they exhibit an armchair pattern along the circumference. A single-wall armchair nanotube is geometrically obtained by rolling up a single graphene layer around y direction according to Fig. 1. The length of circumference of armchair nanotube is obtained as $\mathcal{R} = an\sqrt{3}$. Now a periodic boundary condition for armchair nanotube (n,n) defines the small number of allowed wave vectors k_x in the circumferential direction,

$$\begin{aligned} \mathrm{e}^{\mathrm{i}k_{x,q}\mathcal{R}} &= \mathrm{e}^{\mathrm{i}2\pi q}, \\ nk_{x,q}a &= 2\pi q \longrightarrow k_{x,q} = \frac{2\pi q}{an\sqrt{3}}. \end{aligned} \quad (4)$$

The integer quantum number q is determined using the first Brillouin zone of honeycomb structure. Based on Fig. 1 and the first Brillouin zone of honeycomb structure, k_x satisfies the expression $-\frac{2\pi}{\sqrt{3}a} < k_x < \frac{2\pi}{\sqrt{3}a}$. Using Eq. (4), one can write $-\frac{2\pi}{\sqrt{3}an} < \frac{2\pi q}{an\sqrt{3}} < \frac{2\pi}{\sqrt{3}an}$. Thus we have $-n < q < n$ for armchair nanotube (n,n). Based on the above statements, we can introduce the wave vector regions for armchair type of nanotubes as follows:

$$k_x = \frac{2\pi q}{an\sqrt{3}} \quad \text{with} \quad -n < q < n, \quad -\frac{4\pi}{3a} < k_y < \frac{4\pi}{3a}. \quad (5)$$

Since each unit cell of armchair graphene structure includes 2 atoms with types A and B, one particle Green's function can be written as the 2×2 matrix. According to the model Hamiltonian introduced in Eq. (2), the elements of noninteracting spin resolved Matsubara Green's function are introduced as the following forms:

$$\begin{aligned} G^{(0)\sigma}_{\mathrm{AA}}(\boldsymbol{k},\tau) &= -\langle\mathcal{T}(a_{\boldsymbol{k},\sigma}(\tau)a^{\dagger}_{\boldsymbol{k},\sigma}(0))\rangle, \\ G^{(0)\sigma}_{\mathrm{AB}}(\boldsymbol{k},\tau) &= -\langle\mathcal{T}(a_{\boldsymbol{k},\sigma}(\tau)b^{\dagger}_{\boldsymbol{k},\sigma}(0))\rangle, \\ G^{(0)\sigma}_{\mathrm{BA}}(\boldsymbol{k},\tau) &= -\langle\mathcal{T}(b_{\boldsymbol{k},\sigma}(\tau)a^{\dagger}_{\boldsymbol{k},\sigma}(0))\rangle, \\ G^{(0)\sigma}_{\mathrm{BB}}(\boldsymbol{k},\tau) &= -\langle\mathcal{T}(b_{\boldsymbol{k},\sigma}(\tau)b^{\dagger}_{\boldsymbol{k},\sigma}(0))\rangle, \end{aligned} \quad (6)$$

where τ is the imaginary time. Symbol $\mathcal{T}$ implies time ordering operator. The Fourier transformation of each Green's function element is obtained by

$$G^{(0)\sigma}_{\alpha\beta}(\boldsymbol{k},\mathrm{i}\omega_n) = \int_0^{1/k_{\mathrm{B}}T}\mathrm{d}\tau\,\mathrm{e}^{\mathrm{i}\omega_m\tau}G^{(0)\sigma}_{\alpha\beta}(\boldsymbol{k},\tau), \quad \alpha,\beta = \mathrm{A},\mathrm{B}, \quad (7)$$

where $\omega_n = (2n+1)\pi k_{\mathrm{B}}T$ is fermionic Matsubara frequency. T introduces the equilibrium temperature of the system. After some algebraic calculation, the following expression is obtained for Green's functions in Fourier presentation

$$\begin{aligned} G^{(0)\sigma}_{\alpha\beta}(\boldsymbol{k},\mathrm{i}\omega_n) &= \sum_{\eta=\pm}\frac{\mathcal{C}^{\alpha\beta}_{\eta,\sigma}(\boldsymbol{k})}{\mathrm{i}\omega_n - E^{\sigma}_{\eta}(\boldsymbol{k})}, \\ E^{\sigma}_{\eta=\pm}(\boldsymbol{k}) &= \pm\sqrt{\Delta^2+|\phi_{\boldsymbol{k}}|^2}-\mu_\sigma, \end{aligned} \quad (8)$$

where α and β refer to the each atomic basis of honeycomb lattice, and $E_\eta(\boldsymbol{k})$ is the band structure of gapped graphene-like structure. Moreover coefficients $\mathcal{C}^{\alpha\beta}_{\eta=\pm}(k)$ are given by

$$\begin{aligned} \mathcal{C}^{\mathrm{AA}}_{\eta,\sigma}(\boldsymbol{k}) &= \frac{1}{1+\frac{|\phi_{\boldsymbol{k}}|^2}{(E^{\sigma}_{\eta}(\boldsymbol{k})+\Delta)^2}}, \\ \mathcal{C}^{\mathrm{BB}}_{\eta,\sigma}(\boldsymbol{k}) &= \frac{|\phi_{\boldsymbol{k}}|^2}{(E^{\sigma}_{\eta}(\boldsymbol{k})+\Delta)^2(1+\frac{|\phi_{\boldsymbol{k}}|^2}{(E^{\sigma}_{\eta}(\boldsymbol{k})+\Delta)^2})}, \\ \mathcal{C}^{\mathrm{AB}}_{\eta,\sigma}(\boldsymbol{k}) &= \frac{\phi^*_{\boldsymbol{k}}}{(E^{\sigma}_{\eta}(\boldsymbol{k})+\Delta)(1+\frac{|\phi_{\boldsymbol{k}}|^2}{(E^{\sigma}_{\eta}(\boldsymbol{k})+\Delta)^2})} = \mathcal{C}^{\mathrm{BA}^*}_{\eta,\sigma}(\boldsymbol{k}). \end{aligned} \quad (9)$$

The spin dependence of each component Green's function in Eq. (8) originates from chemical potential μ_σ. This spin dependent chemical potential μ_σ is determined by the concentration of electrons with spin σ (n^{σ}_{e}),

$$\begin{aligned} n^{\sigma}_{\mathrm{e}} &= \int_{-\infty}^{+\infty}\mathrm{d}\mathcal{E}D(\mathcal{E})\frac{1}{\mathrm{e}^{(\mathcal{E}-\mu_\sigma)/k_{\mathrm{B}}T}+1}, \\ D(\mathcal{E}) &\equiv \frac{1}{N}\sum_{\boldsymbol{k},\eta}-2\,\mathrm{Im}\Big(\frac{1}{\mathcal{E}-\eta\sqrt{\Delta^2+|\phi(\boldsymbol{k})|^2}+\mathrm{i}0^+}\Big). \end{aligned} \quad (10)$$

Here $D(\mathcal{E})$ indicates the total density of states of noninteracting nanotube in the presence of gap parameter. To determine μ_σ, we use the definition of spin polarization and total occupation of electrons. Spin polarization is given by $m = |n_\uparrow - n_\downarrow|/n$ and electronic concentration is expressed as $n = n_\uparrow + n_\downarrow$. Based on the values of magnetization m and electronic concentration n, the chemical potential for each spin degree of freedom, μ_σ, can be obtained by means of Eq. (10).

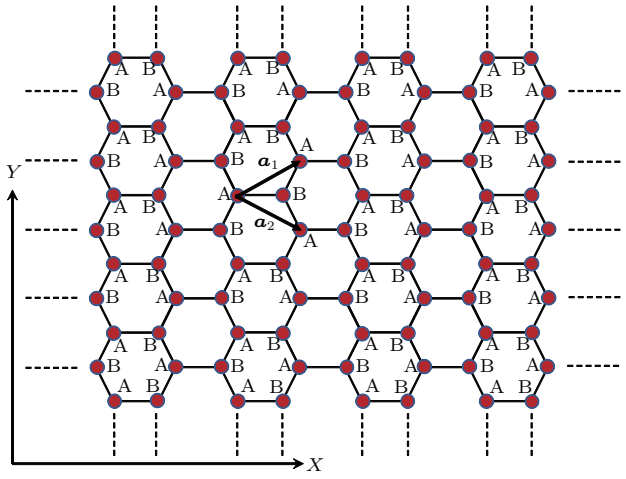


Fig. 1. Crystal structure of honeycomb lattice with two different sublattices. Here $\boldsymbol{a}_1$ and $\boldsymbol{a}_2$ are the primitive unit cell vectors.

The Migdal theorem[32] let us to maintain the lowest order perturbation theory in order to find self energy diagram because phonon energy scale is much smaller in comparison with electronic energy scale. In Holstein phonons, g and $D^{(0)}(\boldsymbol{p}, \mathrm{i}p_m)$ are momentum independent so that the noninteracting phononic propagator is simplified to

$$\begin{aligned} D^{(0)}(\mathrm{i}p_{m'}) &= -\int_0^{1/(k_\mathrm{B}T)} \mathrm{d}\tau \mathrm{e}^{\mathrm{i}p_{m'}\tau} \\ &\quad \times \left\langle T\left(c_{\boldsymbol{k}}(\tau) + c^{\dagger}_{-\boldsymbol{k}}(\tau)\right)\left(c_{\boldsymbol{k}}(0) + c^{\dagger}_{-\boldsymbol{k}}(0)\right)\right\rangle \\ &= \frac{2\omega_0}{(\mathrm{i}p_{m'})^2 - \omega_0^2}, \end{aligned} \tag{11}$$

where $p_{m'} = 2m'\pi k_\mathrm{B}T$ with integer number m' implying the bosonic Matsubara frequency. Due to dispersionless property of Holstein phonon frequency, the off-diagonal elements of self energy matrix get zero value. Since the propagator of phonons in the Holstein model is local, the electronic self-energy is momentum independent. Thus Feynman diagrammatic rules[24] at second order perturbation theory for electron-Holstein phonon interaction gives us the matrix element of spin dependent diagonal self-energy as follows:

$$\begin{aligned} &\Sigma^{\sigma}_{\alpha\alpha}(\mathrm{i}\omega_m) \\ &= -\frac{k_\mathrm{B}T}{N}\sum_{\boldsymbol{k},m'} g^2 D^{(0)}(\mathrm{i}p_{m'}) G^{(0)\sigma}_{\alpha\alpha}(\boldsymbol{k}, \mathrm{i}\omega_m - \mathrm{i}p_{m'}), \end{aligned} \tag{12}$$

where diagonal matrix elements of noninteracting Green's function ($G^{(0)\sigma}_{\alpha\alpha}$) has been replaced in order to calculate self-energy. Since screening effects corresponding to static charge susceptibility[25] have been obtained from electronic density of states at Fermi surface, phononic self-energy is negligible for graphene-like structures approximately. Therefore the propagator of Holstein phonons in Eq. (12) is considered to be unscreened. In order to calculate the summation over internal Matsubara frequency $p_{m'}$, we use Lehman representation[33] as follows:

$$\begin{aligned} &G^{(0)\sigma}_{\alpha\alpha}(\boldsymbol{k}, \mathrm{i}\omega_m - \mathrm{i}p_{m'}) \\ &= \int_{-\infty}^{+\infty} \frac{\mathrm{d}\omega}{2\pi} \frac{-2\mathrm{Im}G^{(0)\sigma}_{\alpha\alpha}(\boldsymbol{k}, \omega + \mathrm{i}0^+)}{\mathrm{i}\omega_m - \mathrm{i}p_{m'} - \omega}. \end{aligned} \tag{13}$$

Substituting Eq. (13) into Eq. (12) and applying the Matsubara frequency summation rules, we can obtain spin-dependent self-energy matrix elements as follows:

$$\begin{aligned} \Sigma^{\sigma}_{\alpha\alpha}(\mathrm{i}\omega_m) &= \frac{g^2}{2N}\sum_{\boldsymbol{k}}\int_{-\infty}^{+\infty}\frac{\mathrm{d}\varepsilon}{2\pi} \\ &\quad \times \left(\frac{n_\mathrm{B}(\omega_0) + n_\mathrm{F}(\varepsilon)}{\mathrm{i}\omega_m - \varepsilon + \omega_0} + \frac{n_\mathrm{B}(\omega_0) + 1 - n_\mathrm{F}(\varepsilon)}{\mathrm{i}\omega_m - \varepsilon - \omega_0}\right) \\ &\quad \times \left(-2\mathrm{Im}G^{(0)\sigma}_{\alpha\alpha}(\boldsymbol{k}, \varepsilon + \mathrm{i}0^+)\right), \end{aligned} \tag{14}$$

with $n_\mathrm{F}(\varepsilon) = \frac{1}{\mathrm{e}^{\beta\varepsilon}+1}$ and $n_\mathrm{B}(\omega_0) = \frac{1}{\mathrm{e}^{\beta\omega_0}-1}$ are Fermi and Bosonic distribution functions, respectively. N denotes the number of unit cells and summation in Eq. (14) is taken over k_x points belonging to the first Brillouin zone of the armchair nanotube. The perturbative expansion for the interacting Green function matrix in the Matsubara notation is given by Dyson's equation[24] as

$$\boldsymbol{G}^{-1}_{\sigma}(\boldsymbol{k}, \mathrm{i}\omega_n) = \boldsymbol{G}^{(0)-1}_{\sigma}(\boldsymbol{k}, \mathrm{i}\omega_n) - \boldsymbol{\Sigma}_{\sigma}(\boldsymbol{k}, \mathrm{i}\omega_n), \tag{15}$$

so that $\boldsymbol{G}_\sigma$ implies Green's function of interacting electrons with spin σ including 2×2 elements. $\boldsymbol{G}^{(0)}_\sigma$ denotes Green's function matrix of tight binding electrons in the presence of magnetic field. The matrix elements of $\boldsymbol{G}^{(0)}_\sigma$ and $\boldsymbol{\Sigma}_\sigma$ have been presented in Eqs. (8) and (14), respectively. The explicit form for each element of interacting Green's function is quite lengthy and is not presented here.

The interesting quantity for studying many particle properties such as plasmon oscillations and phonon softening is the dynamical charge response function. Also this quantity determines the effective electron–electron interaction and the Friedel oscillations. Linear response theory gives us the interacting charge response function (χ) in the presence of quantum effects of electronic interactions based on the correlation function of density-density operators of electron gas (ρ) as

$$\begin{aligned} &\chi(\boldsymbol{q}, \mathrm{i}\Omega_n) = -\sum_\sigma \int_0^{1/k_\mathrm{B}T} \mathrm{d}\tau \mathrm{e}^{\mathrm{i}\Omega_n\tau}\langle T(\rho^\sigma(\boldsymbol{q},\tau)\rho^\sigma(-\boldsymbol{q},0))\rangle, \\ &\rho^\sigma(\boldsymbol{q}) = \frac{1}{N}\sum_{\boldsymbol{k}}\left(a^{\dagger}_{\boldsymbol{k}+\boldsymbol{q},\sigma}a_{\boldsymbol{k},\sigma} + b^{\dagger}_{\boldsymbol{k}+\boldsymbol{q},\sigma}b_{\boldsymbol{k},\sigma}\right), \end{aligned} \tag{16}$$

where $\Omega_n = (2n+1)\pi k_\mathrm{B}T$ denotes the Bosonic Matubara frequency. Moreover $\boldsymbol{q}$ belongs to the First Brillioun zone of armchair nanotube presented in Eq. (5). According to the random phase approximation, the charge response function of interacting electrons on armchair nanotube is expressed in terms of one bubble charge susceptibility,[24,33] i.e. χ_bubble, as the following relation

$$\chi(\boldsymbol{q}, \mathrm{i}\Omega_n) = \frac{\chi_\mathrm{bubble}(\boldsymbol{q}, \mathrm{i}\Omega_n)}{1 - V^{\mathrm{e-e}}\chi_\mathrm{bubble}(\boldsymbol{q}, \mathrm{i}\Omega_n)}, \tag{17}$$

where χ_{bubble} is shown with a single-fermion closed loop.[24] Each line in one bubble Feynman diagram of charge susceptibility is interacting electron propagator. $V^{\text{e-e}}$ implies the Fourier transformation of the effective electron–electron interaction. Here the electrons interact with each other via mediation of phonons. Based on Feynman rules the strength of retarded electron–electron interaction via mediating of phonons is obtained using phononic propagator[24]

$$V^{\text{e-e}} = g^2 D^{(0)}(\omega) = \frac{2g^2\omega_0}{\omega^2 - \omega_0^2}. \tag{18}$$

Note this energy scale $V^{\text{e-e}}$ leads to the binding electrons into local pairs, which occurs when the energy scale is large. This energy scale in this situation is named bipolaron binding energy.[34] Now we should calculate one bubble charge response function $\chi_{\text{bubble}}(\boldsymbol{q}, \mathrm{i}\Omega_n)$ in Eq. (17).

Up to one bubble level and after substitution of operator form of electronic density into Eq. (16), we arrive at the following expression for dynamical charge response function $\chi_{\text{bubble}}(\boldsymbol{q}, \mathrm{i}\Omega_n)$,

$$\begin{aligned}
&\chi_{\text{bubble}}(\boldsymbol{q}, \mathrm{i}\Omega_n) \\
&= -\frac{1}{N^2}\sum_{\boldsymbol{k},\boldsymbol{k}'}\sum_{\sigma}\int_0^{1/k_{\text{B}}T} \mathrm{d}\tau \mathrm{e}^{\mathrm{i}\Omega_n\tau} \\
&\times \left\langle T(a^{\dagger}_{\boldsymbol{k}+\boldsymbol{q},\sigma}(\tau)a_{\boldsymbol{k},\sigma}(\tau) + b^{\dagger}_{\boldsymbol{k}+\boldsymbol{q},\sigma}(\tau)b_{\boldsymbol{k},\sigma}(\tau)) \right. \\
&\times \left. (a^{\dagger}_{\boldsymbol{k}+\boldsymbol{q},\sigma}(0)a_{\boldsymbol{k},\sigma}(0) + b^{\dagger}_{\boldsymbol{k}+\boldsymbol{q},\sigma}(0)b_{\boldsymbol{k},\sigma}(0))\right\rangle.
\end{aligned} \tag{19}$$

The long range magnetic ordering for nanotube leads to the fact that the contribution of electrons with down-spin to the response function is different from that of electrons with up-spin. In order to calculate the correlation function in Eq. (19), the elements of interacting one particle spin dependent Green's function presented in Eq. (15) should be exploited. Wick's theorem has been applied to express the charge response in terms of matrix elements of interacting electronic Green's function in the presence of phonons. Consequently we reach the following expression for the bubble dynamical charge response function χ_{bubble} of electrons on the nanotube structure due to Holstein phonons,

$$\begin{aligned}
\chi_{\text{bubble}}(\boldsymbol{q}, \mathrm{i}\Omega_n) &= \frac{1}{N}\sum_{\boldsymbol{k}}\sum_{\alpha,\beta=A,B}\sum_{\sigma}\int_0^{1/k_{\text{B}}T} \mathrm{d}\tau \mathrm{e}^{\mathrm{i}\Omega_n\tau} \\
&\times G^{\sigma}_{\beta\alpha}(\boldsymbol{k}+\boldsymbol{q}, -\tau)G^{\sigma}_{\alpha\beta}(\boldsymbol{k}, \tau).
\end{aligned} \tag{20}$$

One can rewrite the bubble dynamical polarizability function χ_{bubble} in terms of Fourier transformations of Matsubara's representation of electronic Green's function matrix elements as follows:[24]

$$\begin{aligned}
&\chi_{\text{bubble}}(\boldsymbol{q}, \mathrm{i}\Omega_n) \\
&= \frac{1}{N}\sum_{\boldsymbol{k}}\sum_{\alpha,\beta=A,B}\sum_{\sigma} k_{\text{B}}T\sum_{m} G^{\sigma}_{\beta\alpha}(\boldsymbol{k}+\boldsymbol{q}, \mathrm{i}\Omega_n + \mathrm{i}\omega_m)G^{\sigma}_{\alpha\beta}(\boldsymbol{k}, \mathrm{i}\omega_m).
\end{aligned}$$

In order to perform summation over fermionic Matsubara energies ω_m, we exploit the Lehman representation[33] which relates Matsubara Green's function to the imaginary part of retarded Green's function as

$$G^{\sigma}_{\alpha\beta}(\boldsymbol{k}, \mathrm{i}\omega_m) = \int_{-\infty}^{+\infty}\frac{\mathrm{d}\omega}{2\pi}\frac{-2\mathrm{Im}G^{\sigma}_{\alpha\beta}(\boldsymbol{k}, \omega + \mathrm{i}0^+)}{\mathrm{i}\omega_m - \omega}. \tag{21}$$

Substituting the Lehman representations of Matsubara Green's function into Eq. (21) yields the result for χ_{bubble} as follows:

$$\begin{aligned}
&\chi_{\text{bubble}}(\boldsymbol{q}, \mathrm{i}\Omega_n) \\
&= \frac{4}{N}\sum_{\boldsymbol{k}}\sum_{\alpha,\beta}\sum_{\sigma}\int_{-\infty}^{+\infty}\frac{\mathrm{d}\varepsilon}{2\pi}\int_{-\infty}^{+\infty}\frac{\mathrm{d}\varepsilon'}{2\pi}\left(\mathrm{Im}G^{\sigma}_{\beta\alpha}(\boldsymbol{k}+\boldsymbol{q}, \varepsilon + \mathrm{i}0^+)\right) \\
&\times \left(\mathrm{Im}G^{\sigma}_{\alpha\beta}(\boldsymbol{k}, \varepsilon' + \mathrm{i}0^+)\right)k_{\text{B}}T \\
&\times \sum_{m}\frac{1}{(\mathrm{i}\Omega_n + \mathrm{i}\omega_m - \varepsilon)}\frac{1}{(\mathrm{i}\omega_m - \varepsilon')}.
\end{aligned} \tag{22}$$

After frequency summation over fermionic Matsubara frequency ω_m, the bubble dynamical charge susceptibility of electrons on the armchair nanotube lattice takes the following form:

$$\begin{aligned}
&\chi_{\text{bubble}}(\boldsymbol{q}, \mathrm{i}\Omega_n) \\
&= \frac{4}{N}\sum_{\boldsymbol{k}}\sum_{\alpha,\beta}\sum_{\sigma}\int_{-\infty}^{+\infty}\frac{\mathrm{d}\varepsilon}{2\pi}\int_{-\infty}^{+\infty}\frac{\mathrm{d}\varepsilon'}{2\pi}\left(\mathrm{Im}G^{\sigma}_{\beta\alpha}(\boldsymbol{k}+\boldsymbol{q}, \varepsilon + \mathrm{i}0^+)\right) \\
&\times \left(\mathrm{Im}G^{\sigma}_{\alpha\beta}(\boldsymbol{k}, \varepsilon' + \mathrm{i}0^+)\right)\frac{n_{\text{F}}(\varepsilon) - n_{\text{F}}(\varepsilon')}{\mathrm{i}\Omega_n + \varepsilon - \varepsilon'},
\end{aligned} \tag{23}$$

where $n_{\text{F}}(x) = \frac{1}{\mathrm{e}^{x/k_{\text{B}}T}+1}$ is the Fermi–Dirac distribution function. Notice that the frequency of collective charge modes are determined by finding the position of peaks in the imaginary part of retarded form of dynamical charge susceptibility. Using Eq. (17) and effective electron–electron interaction presented in Eq. (18), the imaginary part of retarded charge susceptibility of interacting electrons is found by analytic continuation $\mathrm{i}\Omega_n \longrightarrow \omega + \mathrm{i}0^+$,

$$\begin{aligned}
&\mathrm{Im}\,\chi(\boldsymbol{q}, \mathrm{i}\Omega_n \longrightarrow \omega + \mathrm{i}0^+) \\
&= \mathrm{Im}\left(\frac{\chi_{\text{bubble}}(\boldsymbol{q}, \mathrm{i}\Omega_n \longrightarrow \omega + \mathrm{i}0^+)}{1 - \frac{2g^2\omega_0}{\omega^2 - \omega_0^2}\chi_{\text{bubble}}(\boldsymbol{q}, \mathrm{i}\Omega_n \longrightarrow \omega + \mathrm{i}0^+)}\right).
\end{aligned} \tag{24}$$

Static charge structure factor ($S(\boldsymbol{q})$) which is a measure of long range charge ordering for electron density can be related to imaginary part of retarded dynamical charge susceptibility, i.e. $\mathrm{Im}\,\chi(\boldsymbol{q}, \omega)$, using the following relation:

$$\begin{aligned}
S(\boldsymbol{q}, T) &= \sum_{\sigma}\langle\rho^{\sigma}(\boldsymbol{q}, \tau)\rho^{\sigma}(-\boldsymbol{q}, 0))\rangle \\
&= k_{\text{B}}T\sum_{n}\frac{1}{2\pi}\int_{-\infty}^{\infty}\mathrm{d}\omega\frac{-2\,\mathrm{Im}\,\chi(\boldsymbol{q}, \mathrm{i}\Omega_n \longrightarrow \omega + \mathrm{i}0^+)}{\mathrm{i}\Omega_n - \omega} \\
&= \int_{-\infty}^{+\infty}\mathrm{d}\omega\frac{n_{\text{B}}(\omega)}{\pi}\,\mathrm{Im}\,\chi(\boldsymbol{q}, \mathrm{i}\Omega_n \longrightarrow \omega + \mathrm{i}0^+),
\end{aligned} \tag{25}$$

where $n_{\rm B}(x) = \frac{1}{{\rm e}^{x/k_{\rm B}T}-1}$ denotes the Bose–Einstein distribution function. In the next section, we present the numerical results of both dynamical and static charge susceptibilities of armchair nanotubes.

3. Numerical results and discussion

In this section, we present our main numerical results for dynamical and static charge susceptibilities of doped armchair nanotubes in the presence of the Holstein phonons and intrinsic magnetization along the plane. The electronic self-energy due to Holstein phonons has been obtained using numerical calculation of Eq. (14). Afterwards the matrix elements of interacting Green's function of electrons have been found based on Eq. (15). Equation (23) gives us the bubble dynamical charge susceptibility of electrons on the armchair graphene nanotube lattice. Finally by substitution of bubble dynamical charge susceptibility into Eq. (24), the imaginary part of interacting dynamical charge polarizability can be calculated. Also the temperature dependence of static charge susceptibility has been readily calculated using Eq. (25). In the following, the frequency behavior of dynamical susceptibilities is studied at characteristic wave number $\boldsymbol{q}_0 = (q_x, q_y) = (2\pi, \pi/\sqrt{3})$. The temperature behavior of static charge response function is also studied at $\boldsymbol{q}_0$. The electron doping effects have been considered for armchair nanotubes with different values of chemical potential. As it has been mentioned in Section 1, the imaginary part of dynamical charge susceptibility corresponds to inelastic cross section of scattering of charged particles from the electrons of the nanotube structure in the presence of electron–phonon coupling and external magnetic field.

Figure 2 presents the frequency behavior of imaginary part of interacting dynamical charge susceptibility of armchair nanotube (5,5) for different gap parameters at zero magnetization for electron–phonon coupling constant $g/t = 0.2$. The normalized temperature has been fixed at $k_{\rm B}T/t = 0.05$. The frequency position of sharp peak in the imaginary part of charge susceptibility describes collective excitation mode or plasmon frequency. The height of peak in imaginary part of dynamical charge response function corresponds to the intensity of scattered beam from the electrons of graphene nanotubes. As shown in Fig. 2, the frequency position of charge excitation mode with high intensity appears at $\omega/t \approx 3.8$ for gap parameter $\Delta/t = 0.8$. The frequency position of charge excitation mode moves to higher frequencies with increase of gap parameter. This arises from the increase of band gap width in density of states with gap parameter. Based on Fig. 2, we can find that the height of sharp peaks reduces with Δ.

We have also studied the effect of chemical potential on plasmon peaks of armchair nanotube (5,5). The frequency dependence of imaginary part of dynamical charge response function of doped armchair graphene for different normalized chemical potentials, namely $\mu/t = 2.6$, 2.7, 2.8, 2.9, for $\Delta/t = 0.8$ has been depicted in Fig. 3. The normalized temperature has been fixed at $k_{\rm B}T/t = 0.05$. A single sharp peak in ${\rm Im}\chi(\boldsymbol{q}_0, \omega)$ at $\omega/t \approx 1.8$ is clearly observed for all values of μ/t. The intensity of this charge collective mode decays with chemical potential, i.e. electron density, due to increase of scattering between electrons. Also the height of sharp peak which relates to intensity of scattered charged particle beam from the sample reduces with increase of chemical potential. Moreover other sharp peaks at $\omega/t \approx 2.1$ with lower intensity compared to the previous sharp peaks are found for all values of chemical potential according to Fig. 3. The height of this peak is approximately independent of chemical potential. For $\mu/t = 2.6$, 2.7, a broad peak with low intensity appears at frequency below 1.5 so that there is no such a peak for the other chemical potentials.

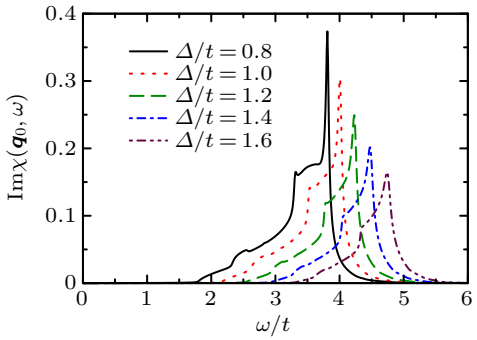


Fig. 2. Imaginary part of dynamical charge susceptibility (${\rm Im}\chi(\boldsymbol{q}_0, \omega)$) of undoped armchair nanotube (5,5) as a function of normalized frequency ω/t for different values of gap parameter Δ/t for fixed temperature $k_{\rm B}T/t = 0.05$. The magnetic field is assumed to be zero. The electron–phonon coupling constant has been fixed as $g/t = 0.2$.

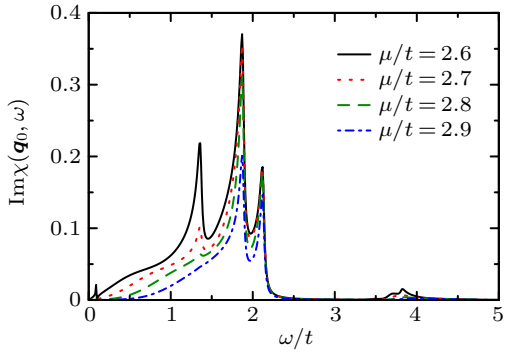


Fig. 3. Imaginary part of dynamical charge susceptibility (${\rm Im}\chi(\boldsymbol{q}_0, \omega)$) of doped armchair nanotube (5,5) as a function of normalized frequency ω/t for different values of chemical potential μ/t for fixed temperature $k_{\rm B}T/t = 0.05$. The magnetization is assumed to be zero. The electron–phonon coupling constant has been fixed as $g/t = 0.2$. The gap parameter has been fixed at $\Delta/t = 0.8$.

In Fig. 4, we have plotted the imaginary part of dynamical charge susceptibility of undoped armchair nanotube (5,5) versus normalized frequency ω/t for different next nearest neighbor hopping amplitudes t'/t, namely $t'/t = 0.24, 0.28, 0.32$. The normalized temperature and coupling constant have been

considered to be $k_{\rm B}T/t = 0.05$ for $g/t = 0.2$, respectively. Also we have fixed normalized gap parameter as $\Delta/t = 0.8$. The higher frequency plasmon modes tend to higher values with t' as shown in Fig. 4.

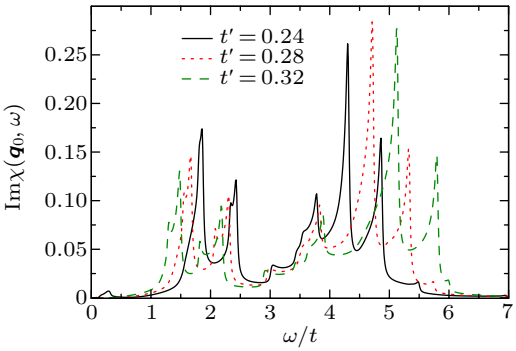


Fig. 4. Imaginary part of dynamical charge susceptibility ($\mathrm{Im}\,\chi(\boldsymbol{q}_0, \omega)$) of undoped armchair nanotube (5,5) as a function of normalized frequency ω/t for different values of next nearest neighbor hopping amplitude t'/t for fixed temperature $k_{\rm B}T/t = 0.05$. The magnetization is assumed to be zero. The electron–phonon coupling constant has been fixed as $g/t = 0.2$. The gap parameter has been fixed at $\Delta/t = 0.8$.

The characteristic results for static charge structure factor ($S(\boldsymbol{q}_0, T)$) of undoped armchair nanotube (5,5) in terms of temperature with different gap parameters, namely $\Delta/t = 0.4, 0.6, 0.8, 1.0$, in the absence of magnetization for electron–phonon coupling constant $g/t = 0.2$ are presented in Fig. 5. There is a peak in the structure factor for each value of Δ so that the temperature position of this peak moves to higher temperature with Δ. This motion of peak position arises from the increase of band gap in density of states with Δ so that the excitation of electrons between bands occurs at higher temperatures. The height of the peak rises with gap parameter. The appearance of peak is an evidence for charge long range ordering. Thus this figure implies the charge ordering increases with ribbon width. A novel feature pronounced in Fig. 5 is the nonzero value for the static structure factor of insulating graphene nanotubes when temperature tends to zero. This result is in contrast to Fermi liquid theory which expresses that the static structure factor at low temperatures is proportional to density of states at Fermi level energy. Therefore the Fermi liquid theory loses its validity for quasi-one-dimensional nanotube system in the presence of electron–phonon coupling. In addition, the static charge structure factor is an evidence for charge ordering of the electronic system. Each curve in Fig. 5 indicates $S(\boldsymbol{q}_0, T)$ increases with temperature until it reaches a maximum and then it exponentially goes to zero. This behavior implies that temperature causes to charge ordering up to maximum point and then more increases of temperature leads to decrease charge ordering.

Also we turn our attention to the effect of electron–phonon coupling strength on the temperature dependence of static structure factor $S(\boldsymbol{q}_0, T)$. In Fig. 6, we have plotted the temperature behavior of $S(\boldsymbol{q}_0, T)$ of undoped armchair nanotube (5,5) for different values of g/t. All the curves in Fig. 6 have a peak at the same value $k_{\rm B}T/t \approx 0.7$ so that the height of peak grows with electron–phonon coupling constant. This increase of height of the peak with g/t corresponds to the increase of charge long range ordering. In fact the localization of electrons rises with increase of electron–phonon coupling strength, which leads to enhancement of charge ordering of electrons. In addition, at fixed values of normalized temperatures below 4, lower g/t causes less localization and consequently lower values in the static structure factor. Moreover it is clearly observed that the structure factor plots on each other on the whole range of temperature above normalized value 4 are shown in Fig. 6. In other words the variation of g/t has no effect on temperature dependence of static structure factor in temperature region $k_{\rm B}T/t > 5$.

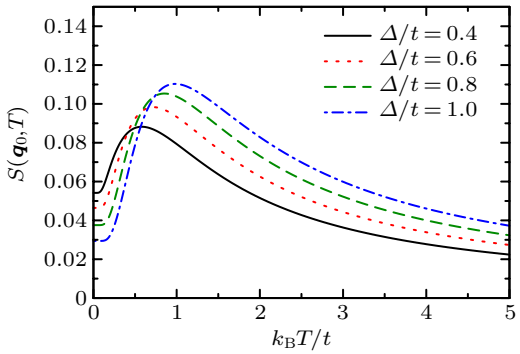


Fig. 5. Static charge susceptibility ($S(\boldsymbol{q}_0, T)$) of undoped armchair nanotube (5,5) as a function of normalized temperature $k_{\rm B}T/t$ for different values of gap parameter Δ/t in the absence of instantanous magnetization. The normalized electron–phonon coupling constant has been fixed as $g/t = 0.05$.

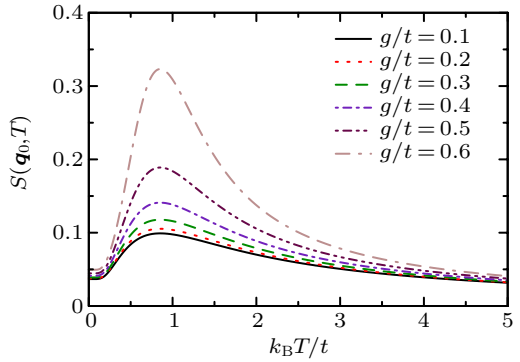


Fig. 6. Static charge susceptibility ($S(\boldsymbol{q}_0, T)$) of undoped armchair nanotube (5,5) as a function of normalized temperature $k_{\rm B}T/t$ for different electron–phonon coupling strength g/t in the absence of instantaneous magnetization. The normalized gap parameter has been fixed as $\Delta/t = 0.8$.

The effect of radial magnetization on temperature dependence of static charge structure factor has been shown in Fig. 7. In this figure we have plotted the temperature dependence of charge structure factor for different values of magnetization, namely $M = 0.0$, 0.009, 0.03, 0.08, for $\Delta/t = 0.8$ with $g/t = 0.2$. The position of the peak in the static structure factor goes to lower values with increase of magnetization. In addition, at fixed value of temperature, the static structure factor enhances with increase of magnetization as shown in Fig. 7.

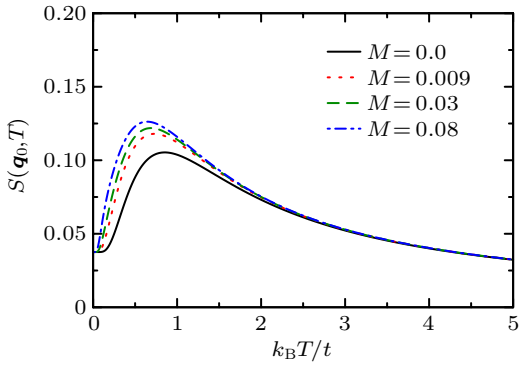


Fig. 7. Static charge susceptibility ($S(\boldsymbol{q}_0,T)$) of undoped armchair nanotube (5,5) as a function of normalized temperature $k_{\rm B}T/t$ for different magnetization values of M at fixed $g/t=0.2$. The normalized gap parameter has been fixed as $\Delta/t=0.8$.

Finally we have studied the effect of chemical potential on temperature dependence of armchair nanotubes in the presence of electron–phonon coupling. In Fig. 8, we have plotted the static charge structure factor $S(\boldsymbol{q}_0,T)$ of the armchair nanotube (5,5) in terms of normalized temperature $k_{\rm B}T/t$ for different values of chemical potential at fixed electron–phonon coupling $g/t=0.2$. The gap parameter has been assumed to be 0.8. For high temperatures above normalized value 3.0, all curves fall on each other, thus static structure factor has no considerable dependence on chemical potential in this temperature region. However, quantum aspects of electrons become important at low temperatures and consequently the structure factor varies with chemical potential. At fixed temperature below normalized value 2.0, the static charge structure factor increases with chemical potential. This implies that the charge long range ordering of electrons improves with increase of chemical potential at low temperatures. In addition, the temperature position of peak in static structure factor moves to lower temperature with chemical potential as shown in Fig. 8. It can be understood from this fact that the charge ordering is preserved at lower temperatures with increase of magnetic field. All the curves indicate a nonzero value for the static structure factor at zero limit of temperature according to Fig. 8.

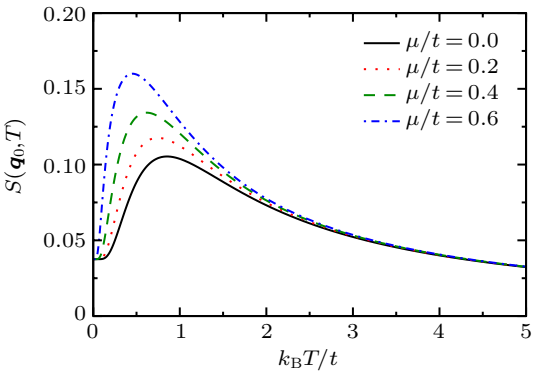


Fig. 8. Static charge susceptibility ($S(\boldsymbol{q}_0,T)$) of undoped armchair nanotube (5,5) as a function of normalized temperature $k_{\rm B}T/t$ for different normalized chemical potential values μ/t at fixed $g/t=0.2$. The normalized gap parameter has been fixed as $\Delta/t=0.8$.

4. Conclusion

In summary, we have studied the effects of both electron phonon interaction and gap parameter on the structure factors and collective magnetic modes of Holstein-model Hamiltonian on the nanotube structure. Using Green's function method, the excitation spectrum of the model hamiltonian has been found. The dynamical charge susceptibility have been calculated using Wick's theorem and excitation spectrum of the model is found. The results show the charge susceptibility includes the sharp well defined peaks in its frequency dependence. Also the behavior of static charge structure factor in terms of chemical potential and temperature has been investigated for different electron phonon coupling strengths.

References

[1] Iijima S 1991 *Nature* **354** 56
[2] Saito R, Dresselhaus G and Dresselhaus M S 1998 *Physical Properties of Carbon Nanotubes* (London: Imperial College Press) p. 305
[3] Hamada N, Sawada S and Oshiyama A 1992 *Phys. Rev. Lett.* **68** 631
[4] Bethune D S, Kiang C H, de Vries M S, Gorman G, Savoy R, Vazquez J, Beyers R 1993 *Nature* **363** 605
[5] Gao L, Zhou X and Ding Y 2007 *Chem. Phys. Lett.* **434** 297
[6] Zhang Y, Wang F C and Zhao Y P 2012 *Comput. Materials Science* **62** 87
[7] Martel R, Schmidt T, Hertel H R and Avouris A R 1998 *Appl. Phys. Lett.* **73** 2447
[8] Derycke V, Martel R, Appenzeller J and Avouris P 2001 *Nano Lett.* **1** 453
[9] Durkop T, Getty S A, Cobas E and Fuhrer M S 2004 *Nano Lett.* **4** 35
[10] Aktruck A and Goldman N 2008 *J. Appl. Phys.* **103** 053702
[11] Basko D M and Aleiner I L 2008 *Phys. Rev. B* **77** 041409
[12] Park C H, Giustino F, Cohen M L and Louie S G 2008 *Nano Lett.* **8** 4229
[13] Su W P, Schrieffer J R and Heeger A J 1979 *Phys. Rev. Lett.* **42** 1698
[14] Holstein T 1959 *Ann. Phys. (N. Y)* **8** 325
[15] Capone M, Ciuchi S 2003 *Phys. Rev. Lett.* **91** 186405
[16] Piscanec S *et al.* 2004 *Phys. Rev. Lett.* **93** 185503
[17] Piscanec S *et al.* 2015 *Phys. Rev. B* **75** 035427
[18] Sasaki K, Sato K, Jiang J, Saito J, Onari S and Tanaka Y 2007 *Phys. Rev. B* **75** 235430
[19] Doniach S and Sondheimer E H 1999 *Green's Functions for Solid State Physicists* (London: Imperial College Press) p. 205
[20] Liu Y and Willis R F 2010 *Phys. Rev. B* **81** 081406
[21] Matz R and Luth H 1981 *Phys. Rev. Lett.* **46** 500
[22] Jalabert R and Das Sarma S 1989 *Phys. Rev. B* **40** 9723
[23] Hwang E H and Sarma S 1995 *Phys. Rev. B* **52** R8668
[24] Mahan G D 1993 *Many Particle Physics* (New York: Plenumn Press) p. 310
[25] Grosso G, Parravincini G P 2003 *Solid State Physics* (New York: Academic Press) p. 108
[26] Ando T 2006 *J. Phys. Soc. Jpn.* **75** 074716
[27] Stauber T, Peres N M and Guinea F 2007 *Phys. Rev. B* **76** 205423
[28] Castro A, Neto H and Guinea F 2007 *Phys. Rev. B* **75** 045404
[29] Pyatkovskiy P K 2009 *J. Phys.: Condens. Matter* **21** 025506
[30] Roldan R, Fuchs J N and Georbig M O 2009 *Phys. Rev. B* **80** 085408
[31] Ramezanali M R, Vazifeh M M, Asgari R, Polini M and Macdonald A H 2009 *J. Phys. A: Math. Theor.* **42** 214015
[32] Migdal A B and Eksp Z 1958 *Teor. Fiz.* **34** 1438
[33] Bruus H, Flensberg K 2004 *Many Body Quantum Theory in Condensed Matter Physics* (Oxford: Oxford University Press) p. 215
[34] Micnas R, Ranninger J and Robaszkiewicz S 1990 *Rev. Mod. Phys.* **62** 113